Desalination and Water Treatment
www.deswater.com
doi: 10.5004/dwt.2022.28971

277 (2022) 155–168
November

Removal of diclofenac, ciprofloxacin and sulfamethoxazole from wastewater using granular activated carbon from hazelnut shell: isotherm, kinetic and thermodynamic studies

Seda Tünay[a], Rabia Köklü[a,*], Mustafa İmamoğlu[b,*]

[a]*Environmental Engineering Department, Faculty of Engineering, Sakarya University, 54050 Sakarya, Turkey, emails: rkoklu@sakarya.edu.tr (R. Köklü), setunse@gmail.com (S. Tünay)*
[b]*Chemistry Department, Faculty of Sciences, Sakarya University, 54050 Sakarya, Turkey, email: imamoglu@sakarya.edu.tr*

Received 6 July 2022; Accepted 6 October 2022

ABSTRACT

The purpose of this study is to determine the effectiveness of phosphoric acid activated hazelnut shell carbon (HSAC) in removing diclofenac (DC), ciprofloxacin (CIP) and sulfamethoxazole (SMX) from aqueous solutions and wastewater. Scanning electron microscopy studies showed that HSAC surface contains numerous irregular pits of various sizes and shapes. The Brunauer–Emmett–Teller surface area of HSAC was found to be 1,173 $m^2 \cdot g^{-1}$. The effect of several parameters including pH, contact time, initial concentration, dosage and temperature on the batch adsorption of DC, CIP and SMX were investigated. Langmuir, Freundlich, Temkin, and Dubinin–Radushkevich isotherms were used to model the adsorption equilibrium of DC, CIP and SMX. The Langmuir isotherm was found to be compatible with the adsorption of DC, CIP and SMX onto HSAC, with maximum adsorption capacities of 125, 95.2 and 285.7 $mg \cdot g^{-1}$ for DC, CIP and SMX, respectively. The pseudo-second-order model was determined to be the most appropriate kinetic model for the adsorption of DC, CIP and SMX. Thermodynamic studies revealed that the adsorption of DC, CIP and SMX onto HSAC was spontaneous and endothermic. The results indicated that HSAC was an easily available, ecofriendly and effective adsorbent for the removal of DC, CIP and SMX from wastewater.

Keywords: Adsorption; Diclofenac; Ciprofloxacin; Sulfamethoxazole; Hazelnut shell; Activated carbon

1. Introduction

All living organisms require water to survive, and therefore, water is considered second of the most valuable resource on the earth after air [1]. Surface waters have frequently been used as a source of drinking water in areas with an expanding urban population [2]. However, as a result of excessive use of chemicals for domestic, industrial and agricultural purposes, surface waters have been polluted [3]. Detection of micro-pollutants such as pharmaceuticals, endocrine disruptors (EDCs) and pesticides in the surface waters has been a serious concern in recent years [2–5].

The pharmaceuticals infiltrate surface waters, drinking waters and ground waters via effluent discharge of wastewater treatment plants due to the incomplete elimination of the pharmaceuticals using conventional treatment processes. The pharmaceuticals or their metabolites can be found at trace level (nanogram to microgram per liter) in the wastewater effluents [4,5]. Even though only trace levels of pharmaceuticals in environment, this results in continuous exposure of on-target organisms via bioaccumulation in aquatic species and the food chain [5]. Pharmaceuticals such as diclofenac (DC) for treatment of rheumatoid arthritis [3,6,7], sulfamethoxazole (SMX) for treatment of bacterial infections [8] and ciprofloxacin (CIP) for treatment

* Corresponding authors.

of urinary tract infections [9] have been widely used by patients and mostly detected in aquatic environments having ecotoxic effects on a wide variety of organisms in the environment [6–9].

Removal methods of the pharmaceuticals from the aquatic environment include adsorption [10], ultrafiltration, nanofiltration, reverse osmosis [11] membrane bioreactors [12], photocatalytic degradation [13], advanced oxidation [14] and degradation by ultrasonic irradiation [15]. Among the different available methods, the adsorption is commonly utilized for the removal of pollutants such as pharmaceuticals, dyes and heavy metals, due to its relative simplicity, efficiency, economical and environmental friendliness [16–18]. Therefore, the development of new adsorbent materials that are affordable, efficient and easily available becomes critical as an effective removal method in wastewater treatment. Using agricultural wastes to produce activated carbon (AC) is a desirable method because it is relatively cheaper and environmentally friendly as activated carbon precursors, as well as allowing for efficient waste management. Activated carbons were fabricated from a variety of agricultural wastes including orange peel [16], pumpkin peel carbon [18,19], rice hull [20], cherry seeds [21], corn cobs, corn leaves and wheat straw [22], palm shell [23], tamarind shell [24], coconut shell [25], walnut shell [26], hazelnut husk [27,28] and tea leaves [29].

Cheap, locally available and agricultural byproducts are preferred for the production of AC to decrease commercial AC production cost. Hazelnut has been produced in significant quantities in Turkey, Spain, Italy, and USA. Hazelnut production of Turkey is about 750,000 ton/y which is about 60%–80% of the world production. Hazelnut shell (HS) is by product of hazelnut and appeared annually about 375,000 ton. HS could be accepted to be good precursor for AC production due to its low cost, locally available in huge quantities and renewability every year. Other advantages of HS could be listed as low economical value compared some precursor used for AC production such as molasses [30] and wheat bran [31], and no need to workforce for its gathering it is ready material in the field and storability for a long time without deterioration on the contrary of the precursors such as pumpkin peels [18]. Hence, the conversion of waste hazelnut shell to the value added material and investigation its adsorption ability to pharmaceuticals such as DC, CIP and SMX from wastewater is very important. HS based adsorbent materials have been reported in the literature, including such as zero-valent iron@biochar wastes for the adsorptive removal of tetracyclines [32], $KMnO_4$-modified activated carbon for adsorption of U(VI) from aqueous solution [33], biochar for Cu(II) adsorption [34], activated carbon for adsorption of copper(II) ions [35], magnetic biochar for adsorption of Penicillin-G from the contaminated water [36], nano-magnetic activated carbon for adsorption of arsenic and mercury [37], magnetic microporous biochar for removal of p-arsanilic acid [38], activated carbon produced with $ZnCl_2$ activation for CIP adsorption [39] and activated carbon for removal of lead, cadmium, zinc, and copper from industrial wastewater [40]. According to the our literature survey, there was no study on the removal of DC, CIP and SMX using hazelnut shell activated carbon prepared with H_3PO_4 activation.

The purpose of this study was to test DC, CIP and SMX adsorption ability of phosphoric acid activated hazelnut shell carbon (HSAC) from aqueous solutions and wastewater. The produced HSAC was characterized using several techniques including proximate analysis, elemental analysis, Brunauer–Emmett–Teller (BET) surface area measurement, scanning electron microscopy (SEM) images and Fourier-transform infrared spectroscopy (FTIR). Batch adsorption of DC, CIP and SMX by HSAC were conducted to determine the influence of pH, contact time, dose, initial concentration and temperature. Pseudo-first-order, pseudo-second-order and intraparticle diffusion kinetic models were used to study adsorption kinetics of DC, CIP and SMX. Langmuir, Freundlich, Temkin, and Dubinin–Radushkevich isotherm models were used to model the adsorption equilibrium of DC, CIP and SMX onto HSAC. Thermodynamic studies were also conducted to determine the free energy (ΔG), enthalpy (ΔH) and entropy changes (ΔS) for the adsorption of DC, CIP and SMX onto HSAC.

2. Experimental

2.1. Chemicals and instruments

Analytical-grade chemicals and reagents were used in the study. DC and SMX were purchased from Sigma-Aldrich, St. Louis, Missouri, USA. CIP was provided by Deva Holding A.Ş., Istanbul, Turkey. Aqueous stock solutions of DC and CIP at 500 $mg{\cdot}L^{-1}$, and SMX at 200 $mg{\cdot}L^{-1}$ was prepared. The standard and working solutions were daily prepared by the dilution of the stock solution.

An electrical vibratory sieve shaker (Retsch Model AS200, Retsch Technology GmbH, Haan, Germany) was used to determine the particle size of HS and HSAC. A temperature-controlled orbital shaker (KS 4000i, IKA®-Werke GmbH & Co. KG, Staufen, Germany) was utilized to agitate the HSAC–pharmaceutical solution suspensions. The pH of the solutions was adjusted to the desired pH values with HCl (0.1 M) and NaOH (0.1 M) solutions by determination using a Schott CG 840 pH Meter (Schott AG, Mainz, Germany). A UV-Spectrophotometer (Shimadzu UV-2600, Shimadzu Corporation, Kyoto, Japan) was used to determine the equilibrium concentrations of CIP, SMX and DC at wave numbers 276, 285 and 276 nm, respectively. HSAC was produced in a tube furnace (Protherm PTF 12, Alser Teknik Seramik A.Ş., Ankara, Turkey). Scanning electron microscopy (SEM, FEI, Quanta FEG 250, USA) was used to characterize the surface morphology of HSAC at DUBİT, Düzce University, Turkey. The BET surface area determination and non-local density functional theory (NLDFT) pore structure analysis were performed using Quantachrome's Autosorb-6B (Quantachrome Instruments, FL, USA), and C,H,N elemental analysis were performed using a Leco CHNS-932 Analyzer (LECO Corp., MI, USA) at Central Laboratory of Middle East Technical University, Ankara, Turkey. Thermogravimetric analysis (TGA) of the HSAC determined by thermal analysis system (Shimadzu, Model DTG-60H, Shimadzu Corp., Kyoto, Japan). In the simultaneous removal of DC, CIP and SMX from aqueous solutions and real wastewater experiments, the level of DC, CIP and SMX in the solutions before and after adsorption

were determined by a high-performance liquid chromatography (HPLC, LC 20AD Prominence, Shimadzu, Japan) with a C18 column (4.6 mm × 250 mm inner diameter, 5 μm particle size, Shimadzu, Japan) at 298 K. Isocratic elution of acetonitrile/ammonium acetate (0.01 M) was used as a mobile phase in a ratio of 70/30 (v/v) and the flow rate was 1.0 mL·min^{-1}. A UV diode array detector (SPD-M20A, Shimadzu, Japan) running at 276 nm for DC and CIP, and 265 nm for SMX was used to detect the absorption of DC, CIP and SMX in the samples. Calibration was made in the range of 2.5–25 mg·L^{-1}. Retention time of DC, CIP and SMX were 4.95, 2.24 and 2.91 min, respectively.

2.2. Synthesis and characterization of HSAC

The hazelnut shells were rinsed with deionized water, dried overnight at 105°C, and then ground to a size of 1,000–1,500 μm using a steel blender. To prepare AC, equal amounts of H_3PO_4 and HS (150 g) were added to 150 mL of deionized water. After 24 h of the impregnation at 80°C in a water bath, the material was dried for 24 h at 105°C. It was then pyrolyzed at 600°C under N_2 flow (100 mL·min^{-1}) in the tube furnace. After cooling at room temperature under N_2, the obtained material was rinsed multiple times with hot deionized water. It was immersed overnight in a 1% $NaHCO_3$ solution to eliminate any leftover acid and then rinsed with distilled water until the pH of the washing water was 7.0. After drying at 105°C for 24 h, the obtained HSAC was sieved to reach a particle size of 250–500 μm and stored in brown glass bottles for use in the subsequent experiments [18,28].

Proximate analysis was used to characterize HSAC according to the American Society for Testing and Materials (ASTM) standards. The functional groups on the HSAC surface were determined by FTIR between the 450 and 4,000 cm^{-1}. The multipoint surface area of HSAC was calculated using N_2 adsorption–desorption isotherms at 77 K and calculated using the BET method. HSAC's surface morphology was investigated using SEM images. The pH_{PZC} values were determined by adding 0.1 g HSAC to a 0.1 M serial NaCl solution with an initial pH value of between 2 and 12. The pH of the NaCl solutions was adjusted to 0.1 M NaOH or 0.1 M HNO_3. The suspensions were then shaken for 24 h. Then, the equilibrium pH values of the solutions were determined. The differences between the equilibrium and initial pH values (ΔpH) were calculated. The point where the curve obtained by plotting the ΔpH values against the initial pH values intersects the x-axis was determined as the pH_{PZC} value [41]. Lactonic, phenolic and carboxylic groups were quantified for HSAC in mmol by Boehm titration. HSAC was added to the individual NaOH, $NaHCO_3$ and Na_2CO_3 solutions (0.1 M) and then the suspensions were shaken for 24 h at a mixing speed of 400 rpm. Then, the samples were collected in an Erlenmeyer using a vacuum filtration. 20 mL of the filtrate was titrated with 0.1 N HCl [42]. To determine the iodine number of HSAC, three different quantities (0.5, 1 and 2 g) were added to the solution of 5% HCl (10 mL) and the suspensions were boiled for 30 ± 2 s. This mixture was then added to 100 mL of 0.1 N iodine solutions and gently shaken for 30 ± 1 s. The suspensions were then filtered and titrated with a 0.1 N sodium thiosulfate [43].

2.3. Batch adsorption experiments

The adsorption dynamics of DC, CIP and SMX with HSAC were evaluated by batch experiments. The effects of parameters such as contact time, initial concentration, HSAC dosage, pH and temperature were investigated. All the batch adsorption of DC, CIP and SMX were carried out using 50 mL of individual aqueous solutions of DC, CIP and SMX. A known amount of HSAC was added to the DC, CIP and SMX solution at definite concentration and then the suspensions were shaken for predetermined time at 25°C (except of temperature effect studies). The specific conditions for each parameter are listed under figures. Then, the suspensions were separated by centrifugation. The equilibrium concentrations of DC, CIP and SMX were measured using a UV-vis spectrophotometer set to 276 nm for DC and CIP, and 265 nm for SMX. The amounts of the pharmaceutical adsorbed per unit mass of HSAC and the adsorption percentages were calculated using Eqs. (1) and (2), respectively:

$$q_e = \frac{\left(C_0 - C_e\right)\cdot V}{m} \tag{1}$$

$$\text{Adsorption},\% = \frac{\left(C_0 - C_e\right)}{C_0}\cdot 100 \tag{2}$$

where q_e (mg·g^{-1}) is the amounts of the pharmaceuticals adsorbed by HSAC; C_0 and C_e are the pharmaceutical concentrations (mg·L^{-1}) at beginning and equilibrium, respectively; V is the solution volume (L) and m is the mass of HSAC (g) [44].

3. Results and discussion

3.1. Characterization of HSAC

The results of elemental analysis, surface functional groups, proximate analysis, iodine number, pH_{PZC} and BET surface analysis of HSAC are summarized in Table 1. The ash content of HSAC was determined to be 13.5%. High ash content may be due to high concentration activating agent's and inorganic content of hazelnut shell. High ash content of AC's can causes clogging of the pores resulting decrease in the surface area [45]. According to Rodríguez-Mirasol et al. [46], high ash content effectively reduced the surface area and porosity of activated carbon products, while activated carbons with low ash level showed better adsorption capacity. Moisture of HSAC was found to be 6.4%. In the literature, the moisture of AC's derived from hazelnut shell [47], pig manure [4] and pumpkin [20] was found to be 7.84%, 7.7% and 8%, respectively. The volatile matter percentage of HSAC was determined as 10.9%. It was reported that when pyrolysis temperatures increase, the release of volatile compounds also increases, resulting in less carbon production [48]. However, as the concentration of activator increased, the amount of volatile substances

Table 1
Characterization data of HSAC

Parameter	Conditions	Value
Elemental analysis (%)		
C		81.1
H		1.6
N		1.1
Surface functional groups (mmol·g^{-1})		
Carboxylic		0.19
Phenolic		0.51
Lactonic		0.22
Total acidic groups		0.92
Proximate analysis (%)		
Moisture	150°C, 3 h	6.4
Ash	650°C ± 25°C, 6 h	13.5
Volatile matter	950°C ± 25°C, 7 min	10.9
Fixed carbon	By difference	75.6
Water solubility		1.5
Iodine number (mg·g^{-1})		588.8
pH_{pzc}		4.24
BET surface area (m^2·g^{-1})		1,173.0

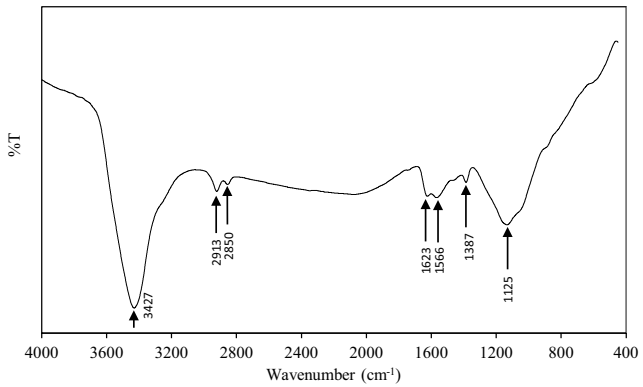

Fig. 1. FTIR spectrum of HSAC.

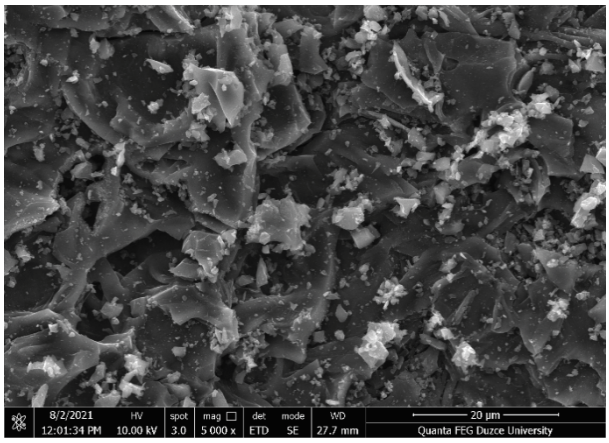

Fig. 2. SEM images of HSAC with 5,000x magnification.

decreased, causing changes in the adsorption properties of activated carbon. Low volatile matter, low moisture and low ash content contributed to the superior quality of activated carbon [49]. Kołodyńska et al. [50] has reported the volatile matter content of cow manure AC as 11.67%.

BET surface area, total pore volume, average pore volume and pore-size distribution of AC's are critical metrics providing important information about AC's adsorption capacity. According to the multi-point BET analysis, the surface area of HSAC was found to be 1,173 m^2·g^{-1}. The surface area of peach seeds AC and hazelnut husk AC were reported to be 1,387.30 [51] and 980.9 m^2·g^{-1} [52], respectively. According to the elemental analysis results, HSAC contains 81.1% C, 1.6% H, 1.1% N. Carbon percentage of pumpkin shell biochar [20], hazelnut shell AC and almond shell AC [53] were reported to be 63%, 51.4% and 49.0%, respectively. The pH_{PZC} value for HSAC was determined as 4.24, indicating that it is neutral at pH 4.24, cationic at pH < 4.24, and anionic at pH > 4.24. Baccar et al. [54] has stated that the pH_{PZC} value of AC is an excellent indicator of the chemical and electronic properties of the surface functional groups.

The FTIR analysis was used to determine the functional groups on the HSAC its surface. The FTIR spectrum of HSAC is shown in Fig. 1. The peak observed at 3427 cm^{-1} could represent O–H stretching vibration of phenolic, alcoholic and acidic functional groups. The absorption peaks at 2923 and 2850 cm^{-1} could be ascribed to the presence of C–H stretching vibration of alkyl groups [55]. The appearance of the peaks around 1623 cm^{-1} could be attributed to the stretching vibration of the aromatic C=C stretching and the lignin structure [56]. The peak observed at 1566 cm^{-1} could be corresponded to the result of C–O stretching. The peak presented at 1387 cm^{-1} could be attributed to the aromatic C–C functional group and/or C–H asymmetric deformation [57]. The peak at 1125 cm^{-1} was indicative of C=O stretching in primary alcohols [58].

The surface morphology of HSAC was determined by SEM examination (Fig. 2). According to the acquired results, numerous irregular pits of various sizes and shapes were discovered randomly distributed on the HSAC surface [59].

N_2 adsorption/desorption isotherm of HSAC are shown in Fig. 3a. According to IUPAC classification, the produced isotherm exhibited hysteresis in I(b) and H4 types [60]. Type I isotherms are found in microporous solids with very small outer surfaces. Type I(b) isotherms have been described for materials with a wider range of pore-size distribution, including larger micropores and possibly narrow mesopores (<~2.5 nm). H4-type hysteresis has been frequently reported in micro mesoporous carbons [60]. The pore-size distribution plot in Fig. 3b showed that HSAC has a small pore-size distribution.

Thermogravimetric analysis (TGA) of HSAC is given in Fig. 4. The first weight loss around 100°C may be caused by the thermodesorption of physically adsorbed materials, such as water, hydrocarbons and volatile matters. There was no significant weight loss till 600°C. The second loss between 600°C–1,000°C was a gradual weight loss and may be due to the loss of carbon in the form of CO_2 and CO from surface

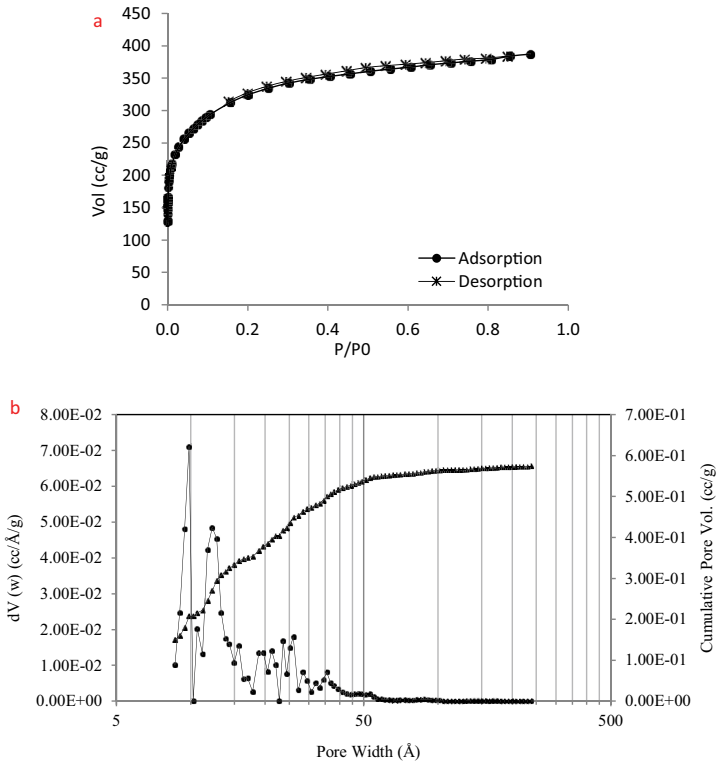

Fig. 3. (a) N_2 adsorption/desorption isotherms of HSAC and (b) pore-size distribution of HSAC.

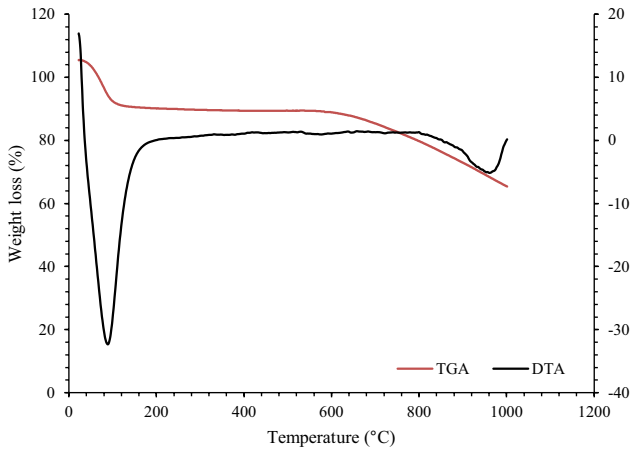

Fig. 4. TG and DTA of HSAC.

oxygen groups, which were formed during oxidation. As shown in the differential thermal analysis (DTA) curve, there was a negative peak at 91.2°C and 966.4°C, indicating that the process was an endothermic process [61,62].

3.2. Effect of initial pH

The pH of the solution is critical in its effect on adsorption performance, since it has a considerable effect on the degree of ionization of the adsorbent's surface functional groups and the adsorbent's surface charge. Additionally, pK_a of the pharmaceuticals is very important for interaction between adsorbent surface functional groups and the pharmaceuticals. The influence of pH on the adsorption of DC, CIP and SMX was investigated in the solution pH range of 6–10 and the experimental findings are given in Fig. 5a. While SMX adsorption is highly affected, DC and CIP adsorption are less affected by pH change of aqueous solution. The DC adsorption onto HSAC was slightly decreased by raising the pH from 6.0 to 10.0. This behavior may be due to increasing negative surface charge of HSAC and deprotonating of DC molecules by raising the pH of aqueous phase [63]. The SMX adsorption onto HSAC sharply decreased by increasing of pH from 6.0 to 7.0 and then the decrease continued to pH 10.0. The decrease in the adsorption of SMX may be due to decrease of electrostatic attraction between HSAC surface and SMX [64]. The adsorbed amount of CIP onto HSAC slowly increased with raising the pH from 6.0 to 10.0. Since CIP was a zwitterionic compound with two pK_a values (pK_{a1} = 6.1; pK_{a2} = 8.7), it exhibited a cationic form at pH < 6.1 and an anionic form at pH > 8.7 due to deprotonation at the carboxylic group. With increasing pH, the partial positive form transformed into the zwitterionic form and the adsorption capacity of CIP increased due to the reduced competition and enhanced electrostatic attraction [65]. In the subsequent adsorption experiments, DC, CIP and SMX solutions at their original pH values was prepared and used.

3.3. Effect of contact time

The variations in the quantity of DC, CIP and SMX adsorbed per gram of HSAC depending on the contact time

are illustrated in Fig. 5b. Adsorption of DC, CIP and SMX was rapid at first, but slowed down after 600 min. This may be due to the fact that initially empty and easily accessible adsorption sites of HSAC were later loaded by DC, CIP and SMX, and so their adsorptions continued in the inner pores of HSAC and required additional time to reach the inner pores [52]. The adsorption of DC, CIP and SMX reached equilibrium at 1,440 min.

3.4. Effect of HSAC dosage

DC, CIP and SMX solutions at a concentration of 200 mg·L^{-1} were mixed for 24 h with HSAC in amounts ranging from 25 to 300 mg to determine the effect of HSAC dosage on the adsorption, and the obtained results are depicted in Fig. 5c. When the HSAC amount was increased from 25 mg to 300 mg, the percent adsorption increased from 26% to 98.5% for DC; 26% to 99.9% for CIP and 62.4% to 99.1% for SMX. Increasing HSAC mass caused in an increase in adsorption zones, resulting in an increase in percent removal. While the adsorption percentage increased, the amount of DC, CIP and SMX adsorbed per gram of HSAC (q_e) decreased due to the inverse relationship between the HSAC dosage and the amount of the pharmaceuticals adsorbed [28,66,67].

3.5. Effect of temperature

Individual DC, CIP and SMX solutions at 100 mg·L^{-1} were mixed with 0.05 g HSAC at 25°C, 35°C and 45°C for 24 h to determine the influence of temperature on the adsorption. The results are shown in Fig. 5d. The adsorption of DC, CIP and SMX onto HSAC increased with

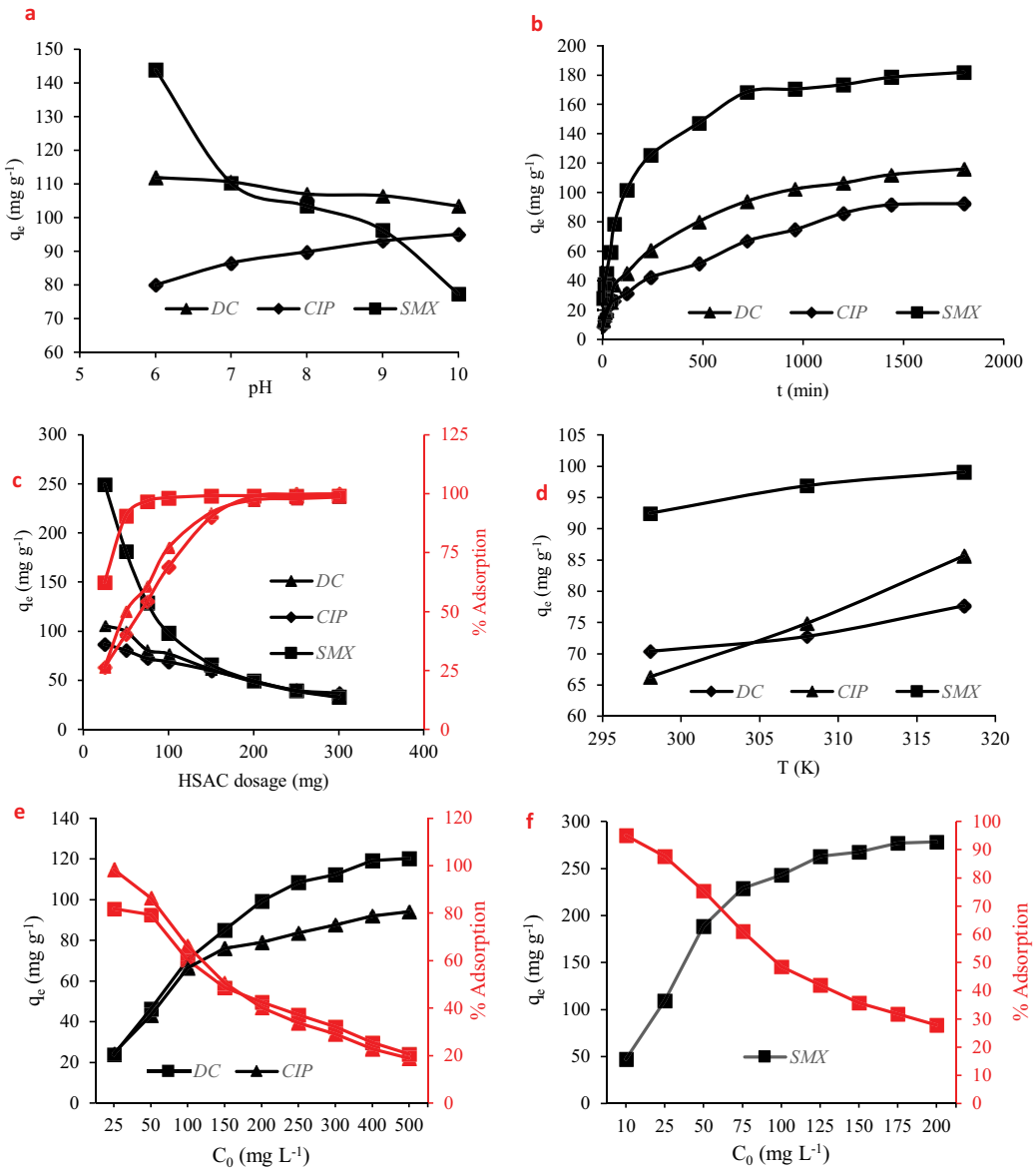

Fig. 5. Effect of parameters the adsorption of DC, CIP and SMX onto HSAC: (a) pH, (b) contact time, (c) HSAC dosage, (d) temperature, (e) initial concentration of DC, CIP and (f) initial concentration of SMX.

increasing temperature showing endothermicity of the process [7,9,32,33]. Similar trends were observed for SMX adsorption with humic acid [68].

3.6. Effect of initial concentration

The effect of the initial concentrations of DC, CIP and SMX on the adsorption onto HSAC is illustrated in Fig. 5e. The adsorbed amount of DC, CIP and SMX onto HSAC increased with the increasing initial concentrations until saturation of HSAC adsorption zones with the adsorbates observed at initial concentrations of 400 mg·L^{-1} for DC and CIP, 175 mg·L^{-1} for SMX. At low initial concentrations of DC, CIP and SMX, there were available empty adsorption zones onto HSAC surface; thus increasing DC, CIP and SMX concentrations caused increases on the adsorbed amounts per gram of HSAC. However, once the adsorption zones on HSAC surface were fully loaded, there were no more available zones for adsorption [44,52]. Hence the adsorption of DC, CIP and SMX did not increase significantly above their initial concentrations of 400 mg·L^{-1} for DC and CIP, 175 mg·L^{-1} for SMX. Additionally, it was observed that the adsorption percentages of DC, CIP and SMX on HSAC decreased as the initial concentrations of DC, CIP and SMX increased.

3.7. Adsorption kinetics by HSAC

In the adsorption processes, the relationship between contact time and adsorption is critical for determining the rate and equilibrium time. The analysis of kinetic data aids in the comprehension of the adsorption mechanism. In this study, the adsorption kinetics of DC, CIP and SMX on HSAC were investigated with pseudo-first-order [69] and pseudo-second-order [70] and intraparticle diffusion [71] models using Eqs. (3) (4) and (5), respectively.

$$\text{Pseudo-first-order: } \ln\left(q_e - q_t\right) = \ln q_e - k_1 t \tag{3}$$

$$\text{Pseudo-second-order: } \frac{t}{q_t} = \frac{1}{k_2 q_e^2} + \frac{t}{q_e} \tag{4}$$

$$\text{Intraparticle diffusion: } q_t = K_{\text{id}} \times t^{1/2} + c \tag{5}$$

where q_e and q_t denote the pharmaceutical quantities adsorbed on HSAC at equilibrium and time t, respectively, and k_1 (min^{-1}) and k_2 (g·mg^{-1}·min^{-1}) denote the pseudo-first-order and pseudo-second-order adsorption rate constants, respectively. The intraparticle diffusion rate constant is K_{id} (mg·g^{-1}·min$^{-1/2}$), while the boundary layer thickness constant is c (mg·g^{-1}). The slope and intercept of the linear curve obtained from the plot $\ln(q_e - q_t)$ vs. t are used to determine the k_1 and $q_{e,\text{cal}}$. The values of $q_{e,\text{cal}}$ and k_2 are determined from the slope and intercept of the t/q_t vs. t plot. The constants K_{id} and c are calculated using the slope and intercept of the q_t vs. $t^{1/2}$ graphs. Table 2 summarizes the calculated kinetic parameters for DC, CIP and SMX adsorption. When the correlation coefficients of the pseudo-first-order and pseudo-second-order models were compared, it was observed that the r^2 values obtained with the pseudo-second-order model for DC, CIP and SMX adsorption was higher and also closer to unity than those obtained with the pseudo-first-order model. When the closeness of the pseudo-second-order model's estimated q_e values ($q_{e,\text{cal}}$) to the empirically determined q_e values ($q_{e,\text{exp}}$) were compared, it was obvious that the pseudo-second-order model's $q_{e,\text{cal}}$ values were closer to the experimental ones. As a result, it was concluded that the pseudo-second-order kinetic model was better appropriate for explaining the adsorption kinetics of DC, CIP and SMX onto HSAC implying that chemical adsorption occurred between the adsorbates and the HSAC surface functional groups [72]. It was reported that the pseudo-second-order kinetic model was more consistent with the adsorption kinetics of CIP on wheat bran-AC [39] and SMX on pine wood-AC [8].

An intraparticle diffusion model was adopted to investigate the adsorption mechanism and to characterize the rate

Table 2
Kinetic parameters for DC, CIP and SMX adsorption on HSAC

Kinetic model	Parameter	Adsorbate		
		DC	CIP	SMX
Pseudo-first-order	$q_{e,\text{exp}}$ (mg·g^{-1})	112.1	91.8	178.6
	k_1 (min^{-1})	2.1 × 10^{-3}	2.5 × 10^{-3}	2.5 × 10^{-3}
	$q_{e,\text{cal}}$ (mg·g^{-1})	97.6	92.6	126.3
	r^2	0.99	0.88	0.98
Pseudo-second-order	k_2 (g·mg^{-1}·min^{-1})	6.3 × 10^{-5}	6.3 × 10^{-5}	7.2 × 10^{-5}
	$q_{e,\text{cal}}$ (mg·g^{-1})	117.7	93.5	185.2
	r^2	0.99	0.95	0.99
Intraparticle diffusion	$K_{\text{id},1}$ (mg·g^{-1}·min$^{-1/2}$)	3.4	3.6	6.3
	r^2	0.99	0.99	0.96
	c_1 (mg·g^{-1})	6.4	1.1	21.0
	$K_{\text{id},2}$ (mg·g^{-1}·min$^{-1/2}$)	1.6	2.2	0.88
	r^2	0.99	0.99	0.93
	c_2 (mg·g^{-1})	52.1	7.4	144.01

control step. The adsorbate is typically transported from the solution to the adsorbent surface in two or three steps. The first step illustrates the passage of the adsorbate from solution to solid surface (film diffusion). The second-step reflects the adsorbate transition to the interior of adsorbent particles (intraparticle diffusion), and the third step involves molecule adsorption to the interior of adsorbent pores. The final step is extremely fast and thus negligible [29]. As seen in Fig. 6, the adsorption of DC, CIP and SMX on HSAC proceed in two stages: film diffusion and intraparticle diffusion. The figure q_t vs. $t^{0.5}$ for the adsorption of DC, CIP and SMX on HSAC did not pass through the origin, and there were two areas representing two distinct stages in the adsorption process [52]. This demonstrates that intraparticle diffusion was not the only control mechanism; film diffusion also influenced the adsorption [73,74].

3.8. DC, CIP and SMX adsorption isotherms by HSAC

Adsorption isotherms reveal the relationship between q_e and C_e at constant temperature and describe adsorbent–adsorbate interactions. Equilibrium curves obtained from experimental data is critical for designing adsorption processes. The Langmuir, Freundlich, Temkin and Dubinin–Radushkevich isotherm models were used to assess the adsorption equilibrium of DC, CIP and SMX onto HSAC. The linear forms of Langmuir, Freundlich, Temkin and Dubinin–Radushkevich isotherm equations expressed by Eqs. (6)–(9), respectively.

$$\frac{C_e}{q_e} = \frac{C_e}{q_{\max}} + \frac{2}{K_L q_{\max}} \tag{6}$$

$$\log q_e = \frac{1}{n}\log C_e + \log K_F \tag{7}$$

$$q_e = \frac{R \times T}{b}\ln K_T + \frac{R \times T}{b}\ln C_e \tag{8}$$

$$\ln q_e = \ln q_m - \beta \times \varepsilon^2 \tag{9}$$

where C_e (mg·L^{-1}) and q_e (mg·g^{-1}) are the concentration of the pharmaceuticals at equilibrium and the amounts of the pharmaceuticals adsorbed by HSAC, respectively. $q_{\max}$ (mg·g^{-1}) and K_L are the Langmuir constant, which express maximum adsorption capacity, and the equilibrium constant or adsorption energy of the adsorbate–absorbent interaction. The plot of C_e/q_e for the function of C_e enables the determination of the Langmuir constants. K_F and $1/n$ are the Freundlich constants that represent the adsorption capacity and the intensity of adsorption, respectively [59]. In Temkin isotherm equation, R is the gas constant and T is the absolute temperature. b and K_T are the Temkin isotherm constant and the equilibrium bonding constant (L·g^{-1}) respectively, and could be determined from the graph of q_e vs. lnC_e [75]. In the Dubinin–Radushkevich model [76],

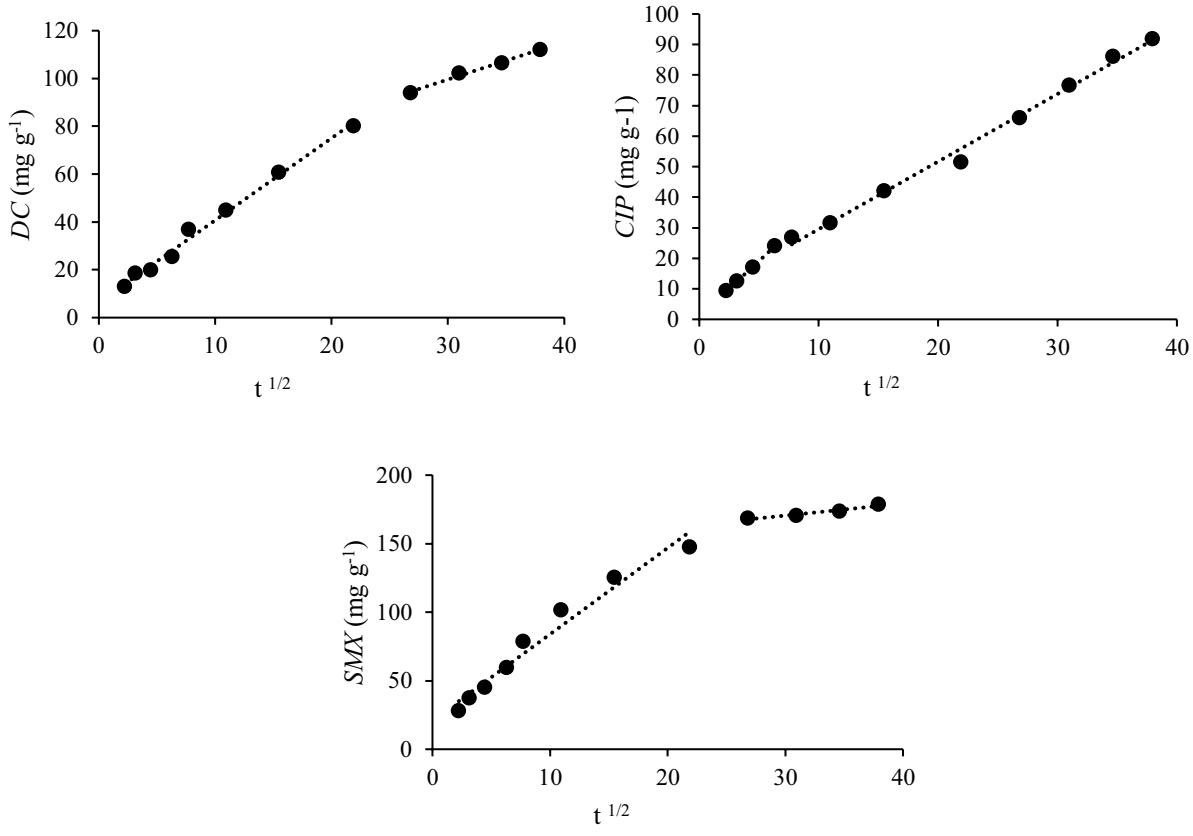

Fig. 6. Intraparticle diffusion model for DC, CIP and SMX adsorption onto HSAC.

β is the isotherm constant associated with the adsorption energy (mol²·kJ²), q_m is the theoretical adsorption capacity (mol·g^{-1}), and ε is the Polanyi potential. ε could be calculated by ε = RT is ln(1 + 1/C_e), where R is gas constant (kJ·mol^{-1}·K^{-1}) and T is temperature (K) [59].

Experimental curves for the adsorption of DC, CIP and SMX with HSAC and the estimated curves by Langmuir, Freundlich, Temkin, and Dubinin–Radushkevich equations are shown in Fig. 7. When the experimentally obtained curve was compared with the predicted curves, the curve anticipated by the Langmuir equation was quite compatible with the experimental ones for DC, CIP and SMX adsorption onto HSAC. Langmuir, Freundlich, Temkin, and Dubinin–Radushkevich constants for adsorption of DC, CIP and SMX with HSAC are listed in Table 3. According correlation coefficients of DC, CIP and SMX adsorption, Langmuir isotherm provides higher correlation coefficients ($r^2 \geq 0.99$) than Freundlich, Temkin, and Dubinin–Radushkevich models. This reveals that the adsorption of DC, CIP and SMX with HSAC was monolayer adsorption that occurs on the homogeneous surface of HSAC [77].

DC, CIP and SMX adsorption capacities by various adsorbents reported in the literature [8,54,72,78–84] were compared with HSAC (Table 4). The DC adsorption capacity of HSAC was higher than olive waste-AC [54] and cocoa pod husk-AC [79]. The CIP adsorption capacity of HSAC was higher than bamboo-AC [81] and sugarcane bagasse-AC [84]. SMX adsorption capacity of HSAC was higher than rice straw-AC [74] and pine tree-AC [8].

A wide variety of methods have been utilized for the removal of DC, CIP and SMX from various water sources, including UV/H_2O_2 [85] for DC, CIP and SMX, nanofiltration [86] for DC and SMX, reverse osmosis [86] for DC and SMX, photocatalytic O_3/UVA/TiO_2 [87] for DC, CuO/TiO_2 ceramic ultrafiltration membrane [88] for CIP, electrochemical oxidation [89] for CIP and Fe-based catalytic ozonation (O_3/Fe^0) [90] for SMX removal. Comparison of the methods reported in the literature with adsorption by HSAC for removal of DC, CIP and SMX are listed in Table 5. The removal of DC by UV/H_2O_2 [85], nanofiltration [86], reverse osmosis [86], photocatalytic O_3/UVA/TiO_2 [87]and HSAC were reported to be >99.0%, 99.7%, 99.9%, 100%, and 94.2%, respectively.

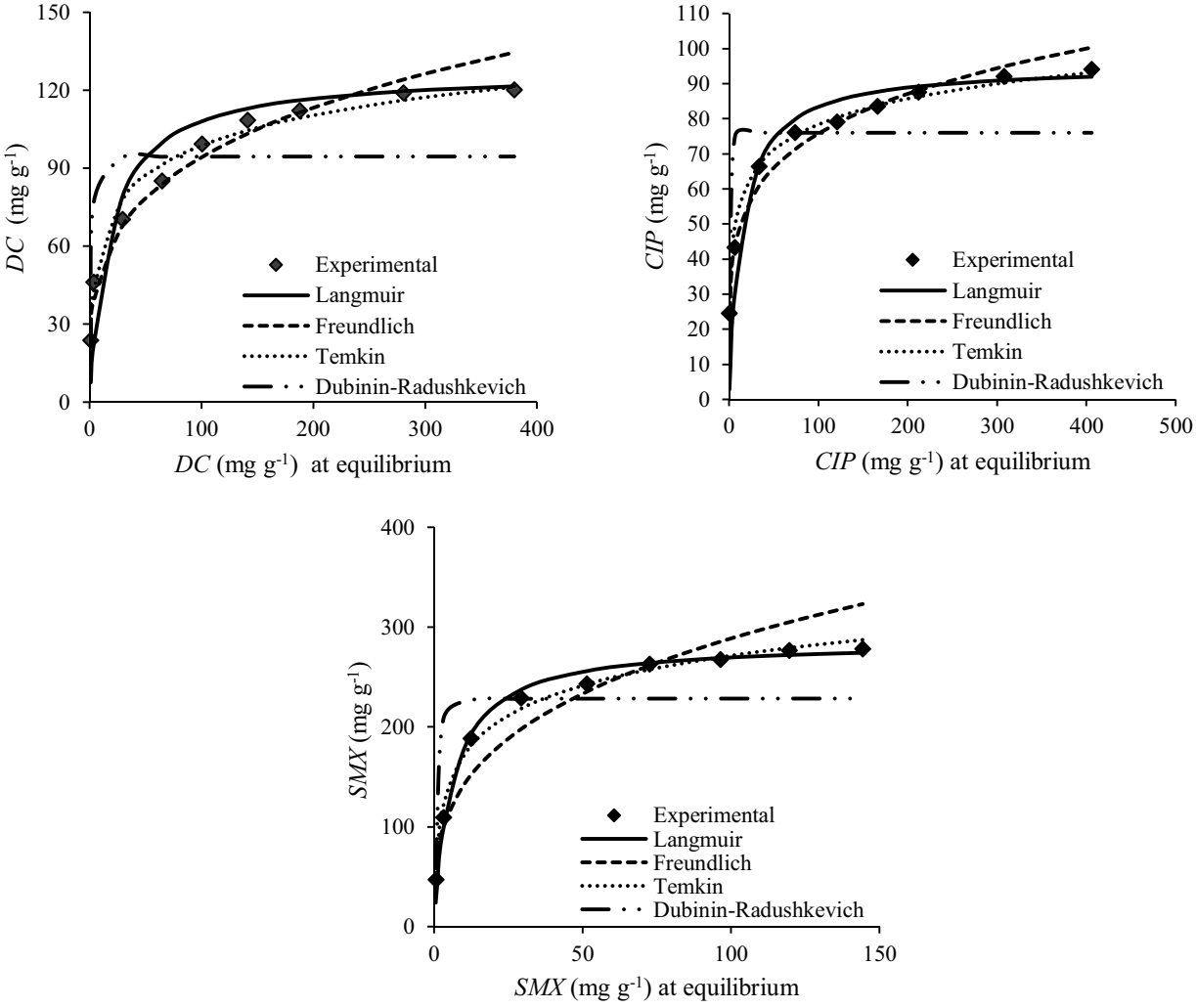

Fig. 7. Experimental and predicted curves by Langmuir, Freundlich, Temkin and Dubinin–Radushkevich models for DC, CIP and SMX adsorption onto HSAC.

Table 3
Parameters of Langmuir and Freundlich isotherms for DC, CIP and SMX adsorption onto HSAC

Isotherm model	Parameter	Adsorbate		
		DC	CIP	SMX
Langmuir	q_{max} (mg·g^{-1})	125.0	95.2	285.7
	K_L (L·mg^{-1})	0.06	0.07	0.17
	r^2	0.99	0.99	0.99
Freundlich	K_F (mg·g^{-1}) (mg·L^{-1})$^{1/n}$	27.4	30.0	70.0
	n	3.73	4.98	3.25
	r^2	0.97	0.99	0.94
Temkin	b	16.98	10.61	43.25
	K_T	3.33	16.00	5.30
	r^2	0.98	0.98	0.99
Dubinin–Radushkevich	q_m (mg·g^{-1})	94.5	76.0	228.4
	β (mmol^2·J^{-2})	3.73	4.98	3.25
	r^2	0.78	0.73	0.80

Table 4
Comparison of DC, CIP and SMX adsorption capacity of HSAC with some other adsorbents reported in the literature

Adsorbent	q_{max} (mg·g^{-1})			References
	DC	CIP	SMX	
Olive waste AC	56.2	–	–	[54]
Rice straw AC	–	–	3.7	[78]
Alligator flag AC	–	–	2	[78]
Cocoa pod husks AC	5.5	–	–	[79]
Pine tree AC	–	–	131	[8]
Peach stones AC	200	–	–	[80]
Bamboo AC	–	36.0	–	[81]
Palm leaves AC	–	133.3	–	[82]
Tea leaves AC	–	238.1	–	[83]
Commercial AC	487	–	–	[63]
Sugarcane bagasse AC	–	9.5	–	[84]
Hazelnut shell AC	125	95.2	285.7	This study

The removal of CIP by UV/H_2O_2 [85], nanofiltration [86], reverse osmosis [86], CuO/TiO_2 ceramic ultrafiltration membrane [88], electrochemical oxidation [89] and HSAC were reported to be >99.0%, 98.1%, 99.8%, 99.5%, 89.5% and 74.8%, respectively. The removal of SMX by UV/H_2O_2 [85], Fe-based catalytic ozonation (O_3/Fe^0) [90] and HSAC were listed to be >99.0%, >99.0% and 73.9%, respectively.

3.9. DC, CIP and SMX adsorption thermodynamics by HSAC

The adsorption thermodynamics of DC, CIP and SMX on HSAC were examined by performing adsorption studies at 25°C, 35°C and 45°C. The investigation on the influence of temperature on the adsorption reveals more precise information regarding thermodynamic parameters such as heat of adsorption (ΔH), entropy change (ΔS) and Gibbs free energy of adsorption (ΔG) [78]. The thermodynamic equations are given by Eqs. (10)–(12).

$$\Delta G = \Delta H - T\Delta S \tag{10}$$

$$\Delta G = -RT\ln K_d \tag{11}$$

$$\ln K_d = -\frac{\Delta H}{RT} + \frac{\Delta S}{R} \tag{12}$$

where R is the universal gas constant (8.314 J·mol^{-1}·K^{-1}) and T is the temperature (K). K_d is the distribution constant calculated by Eq. (13).

$$K_d = \frac{C_a}{C_e} \tag{13}$$

Table 5
Comparison of DC, CIP and SMX adsorption capacity of HSAC with some other removal processes reported in the literature

	Removal process	Removal efficiency	References
Diclofenac	UV/H_2O_2	>99.0	[85]
	Nanofiltration	99.7	[86]
	Reverse osmosis	99.9	[86]
	Photocatalytic O_3/UVA/TiO_2	100	[87]
	HSAC	94.2	This study
Ciprofloxacin	UV/H_2O_2	>99.0	[85]
	Nanofiltration	98.1	[86]
	Reverse osmosis	99.8	[86]
	CuO/TiO_2 ceramic ultrafiltration membrane	99.5	[88]
	Electrochemical oxidation	89.5	[89]
	HSAC	74.8	This study
Sulfamethoxazole	UV/H_2O_2	>99.0	[85]
	Fe-based catalytic ozonation (O_3/Fe^0)	>99.0	[90]
	HSAC	73.9	This study

Table 6
Thermodynamic data for DC, CIP and SMX adsorption onto HSAC

Pharmaceutical	t (°C)	T (K)	K_d	ΔG (kJ·mol^{-1})	ΔH (kJ·mol^{-1})	ΔS (J·mol^{-1}·K^{-1})
	25	298.15	2.37	–2.1		
DC	35	308.15	2.67	–2.5	17.0	63.8
	45	318.15	3.66	–3.4		
	25	298.15	1.96	–1.7		
CIP	35	308.15	2.98	–2.8	43.8	152.0
	45	318.15	5.99	–4.7		
	25	298.15	12.33	–6.2		
SMX	35	308.15	31.25	–8.8	86.1	309.3
	45	318.15	110.11	–12.4		

where C_a is the adsorbed concentration of the pharmaceuticals and C_e is the equilibrium concentration of the pharmaceuticals after their adsorption [78].

For the adsorption of DC, CIP and SMX on HSAC, ΔH and ΔS were computed from the slope and intercept of the plots of lnK_d and 1/T. The calculated thermodynamic parameters are shown in Table 6. Increasing negative values of ΔG imply that the adsorption of DC, CIP and SMX on HSAC occurs spontaneously and is facilitated by increasing the temperature [78]. A positive value for ΔH suggests an endothermicity of DC, CIP and SMX adsorption on HSAC [59]. The ΔH was less than 40 kJ·mol^{-1} suggesting a physisorption process [72,91]. The ΔH of DC adsorption is less than 40 kJ·mol^{-1}, indicating that DC adsorption is of a physical nature. For CIP and SMX adsorptions, the standard enthalpy changes are higher than 40 kJ·mol^{-1}. So, CIP and SMX adsorptions onto HSAC are chemisorption. Positive values of ΔS show an increase in the probability of randomness at the solid–liquid interface during the adsorption of DC, CIP and SMX on HSAC, implying an increase in the system's disorder [59].

3.10. Simultaneous removal of DC, CIP and SMX from aqueous solutions and real wastewater

An aqueous solution containing 10 mg·L^{-1} DC, 10 mg·L^{-1} CIP and 10 mg·L^{-1} SMX was prepared. Various amount of HSAC between 25 and 100 mg were added to the solutions (100 mL) and remaining level of DC, CIP and SMX in the solutions were determined by HPLC. The obtained results are depicted in Fig. 8. When the HSAC amount was increased from 25 to 100 mg, the percent adsorption increased from 69% to 100% for DC; 40.6% to 100% for CIP and 62% to 100% for SMX.

The real wastewater sample was collected from Adapazarı urban wastewater treatment plant of Turkey. The wastewater was spiked with 10 mg·L^{-1} DC, 10 mg·L^{-1} CIP and 10 mg·L^{-1} SMX. The initial concentrations of DC, CIP and SMX were determined by HPLC as 9.5, 10.5 and 11.2 mg·L^{-1}, respectively. HSAC amounts in the range of 25–100 mg were added to 100 mL of the wastewater and the suspensions were shaken for 24 h at ambient temperature. After adsorption, the remaining concentrations of DC, CIP and SMX were measured using HPLC. The obtained results are depicted in Fig. 9. When the HSAC amount was increased from 25 to 100 mg, the percent adsorption increased from 34.98% to 91.41% for DC; 26.94% to 92.76% for CIP and 44.1% to 90.88% for SMX. Overall, HSAC could be accepted as an excellent adsorbent for DC, CIP and SMX removal in real wastewater.

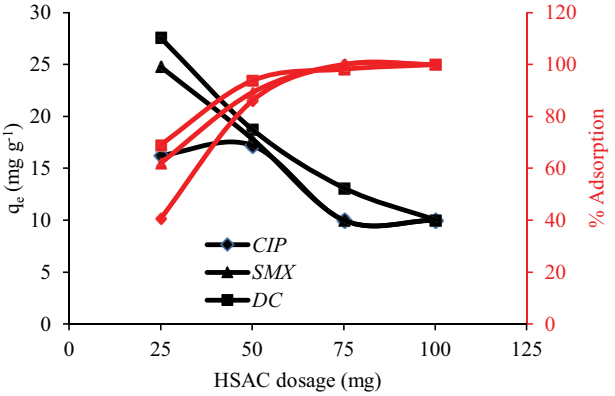

Fig. 8. Simultaneous removal of DC, CIP and SMX from aqueous solutions using HSAC.

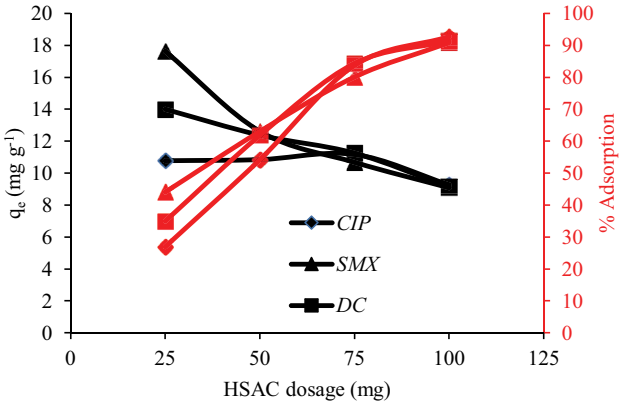

Fig. 9. Removal of DC, CIP and SMX from real wastewater using HSAC.

4. Conclusions

In this study, an activated carbon from hazelnut shell with activation using phosphoric acid was found to be

efficient for removal of DC, CIP and SMX from aqueous solution and wastewater. The AC was easily prepared form waste hazelnut shell with high surface area. Adsorption of DC, CIP and SMX onto HSAC was affected by pH, contact time, initial concentrations of the pharmaceuticals and temperature. The optimum contact period for DC, CIP and SMX was determined to be 1,440 min. Increasing of initial concentrations of DC, CIP and SMX caused an increase the adsorbed amount of the pharmaceutical per gram HSAC. The adsorption equilibriums of DC, CIP and SMX were compatible with the Langmuir isotherm equation. The maximum adsorption capacities of DC, CIP and SMX by HSAC were found to be 125, 95.2 and 285.7 $mg \cdot g^{-1}$. The adsorption kinetic of DC, CIP and SMX followed the pseudo-second-order model. Thermodynamic studies showed that the adsorption of DC, CIP and SMX on HSAC was a spontaneous and endothermic.

In summary, HSAC could be deemed as an efficient, environmentally friendly, easily accessible and low-cost adsorbent for the removal of DC, CIP and SMX from wastewater.

Acknowledgment

The authors thank Deva Holding (Istanbul, Turkey) for supplying ciprofloxacin.

Data availability

The datasets used during the current study are available from the corresponding author on reasonable request.

Author contributions

All authors contributed to the study conception and design. Rabia Köklü founded resources. Mustafa İmamoğlu provided laboratory facilities. HSAC preparation was carried out by Seda Tünay and Mustafa İmamoğlu. Adsorption studies, characterization analyzes, data collection and calculations were performed by Seda Tünay. The first draft of the manuscript was written by Seda Tünay. Rabia Köklü and Mustafa İmamoğlu edited the manuscript. All authors read and approved the final manuscript.

Funding

This work was supported by Sakarya University Research Fund with Project Number: 2019-7-25-260.

Competing interests

The authors declare that they have no completing financial interests or personal relationships that could have appeared to influence the work reported in this paper.

References

[1] D.B. Aulenbach, Water—Our Second Most Important Natural Resource, BC Indus. & Com. L. Rev., 9 (1967) 535.
[2] Y. Yang, X. Zhang, J. Jiang, J. Han, W. Li, X. Li, K.M.Y. Leung, S.A. Snyder, P.J.J. Alvarez, Which micropollutants in water environments deserve more attention globally?, Environ. Sci. Technol., 56 (2021) 13–29.
[3] T.K. Kasonga, M.A.A. Coetzee, I. Kamika, V.M. Ngole-Jeme, M.N.B. Momba, Endocrine-disruptive chemicals as contaminants of emerging concern in wastewater and surface water: a review, J. Environ. Manage., 277 (2021) 111485, doi: 10.1016/j.jenvman.2020.111485.
[4] A. Daneshvar, J. Svanfelt, L. Kronberg, G.A. Weyhenmeyer, Winter accumulation of acidic pharmaceuticals in a Swedish river, Environ. Sci. Pollut. Res. Int., 17 (2010) 908–916.
[5] A. Puckowski, K. Mioduszewska, P. Łukaszewicz, M. Borecka, M. Caban, J. Maszkowska, P. Stepnowski, Bioaccumulation and analytics of pharmaceutical residues in the environment: a review, J. Pharm. Biomed. Anal., 127 (2016) 232–255.
[6] L. Lonappan, S.K. Brar, R.K. Das, M. Verma, R.Y. Surampalli, Diclofenac and its transformation products: environmental occurrence and toxicity - a review, Environ. Int., 96 (2016) 127–138.
[7] P. Higgins, S.H. Siddiqui, R. Kumar, Design of novel graphene oxide/halloysite nanotube@polyaniline nanohybrid for the removal of diclofenac sodium from aqueous solution, Environ. Nanotechnol. Monit. Manage., 17 (2022) 100628, doi: 10.1016/j.enmm.2021.100628.
[8] M. Bizi, Sulfamethoxazole removal from drinking water by activated carbon: kinetics and diffusion process, Molecules, 25 (2020) 4656, doi: 10.3390/molecules25204656.
[9] A. Guellati, R. Maachi, T. Chaabane, A. Darchen, M. Danish, Aluminum dispersed bamboo activated carbon production for effective removal of ciprofloxacin hydrochloride antibiotics: optimization and mechanism study, J. Environ. Manage., 301 (2022) 113765, doi: 10.1016/j.jenvman.2021.113765.
[10] I. Ihsanullah, M.T. Khan, M. Zubair, M. Bilal, M. Sajid, Removal of pharmaceuticals from water using sewage sludge-derived biochar: a review, Chemosphere, 289 (2022) 133196, doi: 10.1016/j.chemosphere.2021.133196.
[11] L. Rizzo, S. Malato, D. Antakyali, V.G. Beretsou, M.B. Đolić, W. Gernjak, G. Mascolo, D. Fatta-Kassinos, Consolidated vs new advanced treatment methods for the removal of contaminants of emerging concern from urban wastewater, Sci. Total Environ., 655 (2019) 986–1008.
[12] T. Gutiérrez-Macías, P. Mijaylova Nacheva, A. Esquivel-Sotelo, L. García-Sánchez, E.B. Estrada-Arriaga, Batch kinetic studies of pharmaceutical compounds removal using activated sludge obtained from a membrane bioreactor, Water Air Soil Pollut., 233 (2022) 36, doi: 10.1007/s11270-022-05508-w.
[13] R.C. Asha, M.P. Yadav, M. Kumar, Sulfamethoxazole removal in membrane photocatalytic reactor system–experimentation and modelling, Environ. Technol., 40 (2018) 1697–1704.
[14] C. Martínez-Sánchez, I. Robles, L.A. Godínez, Review of recent developments in electrochemical advanced oxidation processes: application to remove dyes, pharmaceuticals, and pesticides, Int. J. Environ. Sci. Technol., (2022), doi: 10.1007/s13762-021-03762-9 (In Press).
[15] Y.Q. Gao, J.Q. Zhou, Y.Y. Rao, H. Ning, J. Zhang, J. Shi, N.Y. Gao, Comparative study of degradation of ketoprofen and paracetamol by ultrasonic irradiation: mechanism, toxicity and DBP formation, Ultrason. Sonochem., 82 (2022) 105906, doi: 10.1016/j.ultsonch.2021.105906.
[16] R. Koklu, M. Imamoglu, Removal of ciprofloxacin from aqueous solution by activated carbon prepared from orange peel using zinc chloride, Membr. Water Treat., 13 (2022) 129–137.
[17] M. Imamoglu, Novel determination of copper(II) in natural waters by solid-phase extraction (SPE) flow-injection (FI) flame atomic absorption spectrometry (FAAS), Anal. Lett., (2022), doi: 10.1080/00032719.2022.2092632 (In Press).
[18] Ç. Özer, M. İmamoğlu, Removal of ciprofloxacin from aqueous solutions by pumpkin peel biochar prepared using phosphoric acid, Biomass Convers. Biorefin., (2022), doi: 10.1007/s13399-022-02832-3 (In Press).
[19] D. Bal, Ç. Özer, M. İmamoğlu, Green and ecofriendly biochar preparation from pumpkin peel and its usage as an adsorbent for methylene blue removal from aqueous solutions, Water Air Soil Pollut., 232 (2021) 1–16.
[20] M. Teker, M. Imamoğlu, Ö. Saltabaş, Adsorption of copper and cadmium Ions by activated carbon from rice hulls, Turk. J. Chem., 23 (1999) 185–192.

[21] N. Ozturk, M. Yazar, A. Gundogdu, C. Duran, H.B. Senturk, M. Soylak, Application of cherry laurel seeds activated carbon as a new adsorbent for Cr(VI) removal, Membr. Water Treat., 12 (2021) 11–21.
[22] H. Wei, H. Wang, A. Li, H. Li, D. Cui, M. Dong, J. Lin, J. Fan, J. Zhang, H. Hou, Y. Shi, D. Zhou, Z. Guo, Advanced porous hierarchical activated carbon derived from agricultural wastes toward high performance supercapacitors, J. Alloys Compd., 820 (2020) 153111, doi: 10.1016/j.jallcom.2019.153111.
[23] M. Muniyandi, P. Govindaraj, Potential removal of methylene blue dye from synthetic textile effluent using activated carbon derived from palmyra (Palm) shell, Mater. Today:. Proc., 47 (2021) 299–311.
[24] B.R. Abisha, C.I. Anish, R. Beautlin Nisha, N. Daniel Sam, M. Jaya Rajan, Adsorption and equilibrium studies of methyl orange on tamarind shell activated carbon and their characterization, Phosphorus Sulfur, 197 (2022) 225–230.
[25] L. Wu, X. Zhang, Y. Si, Polydopamine functionalized super-hydrophilic coconut shells biomass carbon for selective cationic dye methylene blue adsorption, Mater. Chem. Phys., 279 (2022) 125767, doi: 10.1016/j.matchemphys.2022.125767.
[26] E. Dovi, A.A. Aryee, A.N. Kani, F.M. Mpatani, J. Li, L. Qu, R. Han, High-capacity amino-functionalized walnut shell for efficient removal of toxic hexavalent chromium ions in batch and column mode, J. Environ. Chem. Eng., 10 (2022) 107292, doi: 10.1016/j.jece.2022.107292.
[27] M. Imamoglu, O. Tekir, Removal of copper(II) and lead(II) ions from aqueous solutions by adsorption on activated carbon from a new precursor hazelnut husks, Desalination, 228 (2008) 108–113.
[28] C. Ozer, M. Imamoglu, Y. Turhan, F. Boysan, Removal of methylene blue from aqueous solutions using phosphoric acid activated carbon produced from hazelnut husks, Toxicol. Environ. Chem., 94 (2012) 1283–1293.
[29] C. Duran, D. Ozdes, A. Gundogdu, M. Imamoglu, H.B. Senturk, Tea-industry waste activated carbon, as a novel adsorbent, for separation, preconcentration and speciation of chromium, Anal. Chim. Acta, 688 (2011) 75–83.
[30] F. Aci, M. Nebioglu, M. Arslan, M. Imamoglu, M. Zengin, M. Kucukislamoglu, Preparation of activated carbon from sugar beet molasses and adsorption of methylene blue, Fresenius Environ. Bull., 17 (2008) 997–1001.
[31] A. Özer, H.B. Pirincci, The adsorption of Cd(II) ions on sulphuric acid-treated wheat bran, J. Hazard. Mater., 137 (2006) 849–855.
[32] D. Hao, Y. Chen, Y. Zhang, N. You, Nanocomposites of zero-valent iron@biochar derived from agricultural wastes for adsorptive removal of tetracyclines, Chemosphere, 284 (2021) 131342, doi: 10.1016/j.chemosphere.2021.131342.
[33] M. Zhu, F. Li, W. Chen, X. Yin, Z. Yi, S. Zhang, Adsorption of U(VI) from aqueous solution by using $KMnO_4$-modified hazelnut shell activated carbon: characterisation and artificial neural network modelling, Environ. Sci. Pollut. Res., 28 (2021) 47354–47366.
[34] B. Zhao, X. Xu, F. Zeng, H. Li, X. Chen, The hierarchical porous structure bio-char assessments produced by co-pyrolysis of municipal sewage sludge and hazelnut shell and Cu(II) adsorption kinetics, Environ. Sci. Pollut. Res., 25 (2018) 19423–19435.
[35] D.D. Milenković, P.V. Dašić, V.B. Veljković, Ultrasound-assisted adsorption of copper(II) ions on hazelnut shell activated carbon, Ultrason. Sonochem., 16 (2009) 557–563.
[36] S. Aghagani, H. Baseri, Production of magnetic biochar from the hazelnut shell and magnetite particles for adsorption of Penicillin-G from the contaminated water, Urban Water J., 19 (2022) 422–432.
[37] M. Zabihi, M. Omidvar, A. Motavalizadehkakhky, R. Zhiani, Competitive adsorption of arsenic and mercury on nano-magnetic activated carbons derived from hazelnut shell, Korean J. Chem. Eng., 39 (2022) 367–376.
[38] Y. Wang, B. Jiang, L. Wang, Z. Feng, H. Fan, T. Sun, Hierarchically structured two-dimensional magnetic microporous biochar derived from hazelnut shell toward effective removal of p-arsanilic acid, Appl. Surf. Sci., 540 (2021) 148372, doi: 10.1016/j.apsusc.2020.148372.
[39] D. Balarak, F.K. Mostafapour, H. Azarpira, Adsorption kinetics and equilibrium of ciprofloxacin from aqueous solutions using *Corylus avellana* (Hazelnut) activated carbon, Br. J. Pharm. Res., 13 (2016) 1–14.
[40] M. Kazemipour, M. Ansari, S. Tajrobehkar, M. Majdzadeh, H.R. Kermani, Removal of lead, cadmium, zinc, and copper from industrial wastewater by carbon developed from walnut, hazelnut, almond, pistachio shell, and apricot stone, J. Hazard. Mater., 150 (2008) 322–327.
[41] W.J. Liu, F.X. Zeng, H. Jiang, X.S. Zhang, Preparation of high adsorption capacity bio-chars from waste biomass, Bioresour. Technol., 102 (2011) 8247–8252.
[42] S. Sivrikaya, S. Albayrak, M. Imamoglu, A. Gundogdu, C. Duran, H. Yildiz, Dehydrated hazelnut husk carbon: a novel sorbent for removal of Ni(II) ions from aqueous solution, Desal. Water Treat., 50 (2012) 2–13.
[43] ASTM, Standard Test Method for Determination of Iodine Number of Activated Carbon, ASTM Annual Book, 1999.
[44] S. Usanmaz, C. Ozer, M. Imamoglu, Removal of Cu(II), Ni(II) and Co(II) ions from aqueous solutions by hazelnut husks carbon activated with phosphoric acid, Desal. Water Treat., 227 (2021) 300–308.
[45] Schröder, K. Thomauske, C. Weber, A. Hornung, V. Tumiatti, Experiments on the generation of activated carbon from biomass, J. Anal. Appl. Pyrolysis, 79 (2007) 106–111.
[46] J. Rodríguez-Mirasol, T. Cordero, J.J. Rodríguez, Preparation and characterization of activated carbons from eucalyptus kraft lignin, Carbon, 31 (1993) 87–95.
[47] M. Kobya, Adsorption kinetic and equilibrium studies of Cr(VI) by hazelnut shell activated carbon, Adsorpt. Sci. Technol., 22 (2004) 51–64.
[48] S.M. Yakout, G.S. El-Deen, Characterization of activated carbon prepared by phosphoric acid activation of olive stones, Arabian J. Chem., 9 (2016) S1155–S1162.
[49] C.E. Brewer, Biochar Characterization and Engineering, Paper 12284, Iowa State University, 2012.
[50] D. Kołodyńska, R. Wnętrzak, J.J. Leahy, M.H.B. Hayes, W. Kwapiński, Z. Hubicki Kinetic and adsorptive characterization of biochar in metal ions removal, Chem. Eng. J., 197 (2012) 295–305.
[51] M. Kobya, E. Demirbas, E. Senturk, M. Ince, Adsorption of heavy metal ions from aqueous solutions by activated carbon prepared from apricot stone, Bioresour. Technol., 96 (2005) 1518–1521.
[52] C. Ozer, M. Imamoglu, Adsorptive transfer of methylene blue from aqueous solutions to hazelnut husk carbon activated with potassium carbonate, Desal. Water Treat., 94 (2017) 236–243.
[53] M. Soleimani, T. Kaghazchi, Agricultural waste conversion to activated carbon by chemical activation with phosphoric acid, Chem. Eng. Technol., 30 (2007) 649–654.
[54] R. Baccar, M. Sarrà, J. Bouzid, M. Feki, P. Blánquez, Removal of pharmaceutical compounds by activated carbon prepared from agricultural by-product, Chem. Eng. J., 211 (2012) 310–317.
[55] D.S. Kumar, P.S. Kumar, N.M. Rajendran, G. Anbuganapathi, Compost maturity assessment using physicochemical, solid-state spectroscopy, and plant bioassay analysis, J. Agric. Food Chem., 61 (2013) 11326–11331.
[56] B. Esteves, A. Velez Marques, I. Domingos, H. Pereira, Chemical changes of heat treated pine and eucalypt wood monitored by FTIR, Maderas-Cienc. Tecnol., 15 (2013) 245–258.
[57] M.E. Saleh, A.A. El-Refaey, A.H. Mahmoud, Effectiveness of sunflower seed husk biochar for removing copper ions from wastewater: a comparative study, Soil Water Res., 11 (2016) 53–63.
[58] P. Lv, G. Almeida, P. Perre, TGA-FTIR analysis of torrefaction of lignocellulosic components (cellulose, xylan, lignin) in isothermal conditions over a wide range of time durations, Bioresources, 10 (2015) 4239–4251.
[59] S. Fan, J. Tang, Y. Wang, H. Li, H. Zhang, J. Tang, Biochar prepared from co-pyrolysis of municipal sewage sludge and tea waste for the adsorption of methylene blue from aqueous solutions: kinetics isotherm thermodynamic and mechanism, J. Mol. Liq., 220 (2016) 432–441.

[60] M. Thommes, K. Kaneko, A.V. Neimark, J.P. Olivier, F. Rodriguez-Reinoso, J. Rouquerol, K.S. Sing, Physisorption of gases with special reference to the evaluation of surface area and pore-size distribution (IUPAC Technical Report), Pure Appl. Chem., 87 (2015) 1051–1069.
[61] R.F.T. Tiegam, D.R.T. Tchuifon, R. Santagata, P.A.K. Nanssou, S.G. Anagho, I. Ionel, S. Ulgiati, Production of activated carbon from cocoa pods: investigating benefits and environmental impacts through analytical chemistry techniques and life cycle assessment, J. Cleaner Prod., 288 (2021) 125464, doi: 10.1016/j.jclepro.2020.125464.
[62] M.M. Maroto-Valer, I. Dranca, T. Upascu, R. Nastas, Effect of adsorbate polarity on thermodesorption profiles from oxidized and metal-impregnated activated carbons, Carbon, 42 (2004) 2655–2659.
[63] B.N. Bhadra, P.W. Seo, S.H. Jhung, Adsorption of diclofenac sodium from water using oxidized activated carbon, Chem. Eng. J., 301 (2016) 27–34.
[64] N. Pamphile, L. Xuejiao, Y. Guangwei, W. Yin, Synthesis of a novel core-shell-structure activated carbon material and its application in sulfamethoxazole adsorption, J. Hazard. Mater., 368 (2019) 602–612.
[65] J. Kong, Y. Zheng, L. Xiao, B. Dai, Y. Meng, Z. Ma, X. Huang, Synthesis and comparison studies of activated carbons based *folium cycas* for ciprofloxacin adsorption, Colloids Surf., A, 606 (2020) 125519, doi: 10.1016/j.colsurfa.2020.125519.
[66] Ç. Özer, M. İmamoğlu, Isolation of nickel(II) and lead(II) from aqueous solution by sulfuric acid prepared pumpkin peel biochar, Anal. Lett., (2022), doi: 10.1080/00032719.2022.2078981 (In Press).
[67] A. Gündoğdu, H.B. Şentürk, C. Duran, M. İmamoğlu, M. Soylak, A new low-cost activated carbon produced from tea-industry waste for removal of Cu(II) ions from aqueous solution: equilibrium, kinetic and thermodynamic evaluation, Karadeniz Chem. Sci. Technol., 2 (2018) 1–10.
[68] X. Liu, S. Lu, Y. Liu, W. Meng, B. Zheng, Adsorption of sulfamethoxazole (SMZ) and ciprofloxacin (CIP) by humic acid (HA): characteristics and mechanism, RSC Adv., 7 (2017) 50449–50458.
[69] S. Lagergren, About the theory of so-called adsorption of soluble substances, Kongl. Vetensk. Acad. Handl., 24 (1898) 1–39.
[70] Y.S. Ho, G. Mckay, Pseudo-second order model for sorption processes, Process Biochem., 34 (1999) 451–465.
[71] W.J. Weber Jr., J.C. Morris, Kinetics of adsorption on carbon from solution, J. Sanit. Eng. Div., 89 (1963) 31–59.
[72] M. Antunes, V.I. Esteves, R. Guégan, J.S. Crespo, A.N. Fernandes, M. Giovanela, Removal of diclofenac sodium from aqueous solution by Isabel grape bagasse, Chem. Eng. J., 192 (2012) 114–121.
[73] A. Gundogdu, C. Duran, H.B. Senturk, M. Soylak, D. Ozdes, H. Serencam, M. Imamoglu, Adsorption of phenol from aqueous solution on a low-cost activated carbon produced from tea industry waste: equilibrium, kinetic, and thermodynamic study, J. Chem. Eng. Data, 57 (2012) 2733–2743.
[74] G. Karaçetin, S. Sivrikaya, M. Imamoglu, Adsorption of methylene blue from aqueous solutions by activated carbon prepared from hazelnut husk using zinc chloride, J. Anal. Appl. Pyrolysis, 110 (2014) 270–276.
[75] M.J. Temkin, V. Pyzhev, Recent modifications to Langmuir isotherms, Acta Physiochim. USSR, 12 (1940) 217–222.
[76] M.M. Dubinin, L.V. Radushkevich, Evaluation of microporous materials with a new isotherm, In Dokl. Akad. Nauk., SSSR, 55 (1947) 331–334.
[77] Z. Shirani, C. Santhosh, J. Iqbal, A. Bhatnagar, Waste *Moringa oleifera* seed pods as green sorbent for efficient removal of toxic aquatic pollutants, J. Environ. Manage., 227 (2018) 95–106.
[78] T. Li, X. Han, C. Liang, M.J.I. Shohag, X. Yang, Sorption of sulphamethoxazole by the biochars derived from rice straw and alligator flag, Environ. Technol., 36 (2015) 245–253.
[79] M.D.G. De Luna, W. Budianta, K.K.P. Rivera, R.O. Arazo, Removal of sodium diclofenac from aqueous solution by adsorbents derived from cocoa pod husks, J. Environ. Chem. Eng., 5 (2017) 1465–1474.
[80] S.A. Torrellas, R.G. Lovera, N. Escalona, C. Sepulveda, J.L. Sotelo, J. Garcia, Chemical-activated carbons from peach stones for the adsorption of emerging contaminants in aqueous solutions, Chem. Eng. J., 279 (2015) 788–798.
[81] L. Wang, G. Chen, C. Ling, J. Zhang, K. Szerlag, Adsorption of ciprofloxacin on to bamboo charcoal: effects of pH, salinity, cations, and phosphate, Environ. Prog. Sustainable Energy, 36 (2017) 1108–1115.
[82] E.S.I. El-Shafey, H. Al-Lawati, A.S. Al-Sumri, Ciprofloxacin adsorption from aqueous solution onto chemically prepared carbon from date palm leaflets, J. Environ. Sci., 24 (2012) 1579–1586.
[83] J. Li, G. Yu, L. Pan, C. Li, F. You, S. Xie, Y. Wang, J. Ma, X. Shang, Study of ciprofloxacin removal by biochar obtained from used tea leaves, J. Environ. Sci., 73 (2018) 20–30.
[84] M.E. Penafiel, J.M. Matesanz, E. Vanegas, D. Bermejo, R. Mosteoö, M.P. Ormad, Comparative adsorption of ciprofloxacin on sugarcane bagasse from Ecuador and on commercial powdered activated carbon, Sci. Total Environ., 750 (2021) 141498, doi: 10.1016/j.scitotenv.2020.141498.
[85] C. Afonso-Olivares, C. Fernández-Rodríguez, R.J. Ojeda-González, Z. Sosa-Ferrera, J.J. Santana-Rodríguez, J.D. Rodríguez, Estimation of kinetic parameters and UV doses necessary to remove twenty-three pharmaceuticals from pre-treated urban wastewater by UV/H_2O_2, J. Photochem. Photobiol., A, 329 (2016) 130–138.
[86] S. Beier, S. Köster, K. Veltmann, H. Schröder, J. Pinnekamp, Treatment of hospital wastewater effluent by nanofiltration and reverse osmosis, Water Sci. Technol., 61 (2010) 1691–1698.
[87] A. Aguinaco, F.J. Beltrán, J.F. García-Araya, A. Oropesa, Photocatalytic ozonation to remove the pharmaceutical diclofenac from water: influence of variables, Chem. Eng. J., 189 (2012) 275–282.
[88] P. Bhattacharya, D. Mukherjee, S. Dey, S. Ghosh, S. Banerjee, Development and performance evaluation of a novel CuO/TiO_2 ceramic ultrafiltration membrane for ciprofloxacin removal, Mater. Chem. Phys., 229 (2019) 106–116.
[89] I. Firdaus, A. Yaqub, H. Ajab, I. Khan, B.A.Z. Amin, A. Baig, M.H. Isa, Electrochemical oxidation of amoxicillin, ciprofloxacin and erythromycin in water: effect of experimental factors on COD removal, Pak. J. Pharm. Sci., 34 (2021) 119–128.
[90] N. Shahmahdi, R. Dehghanzadeh, H. Aslani, S.B. Shokouhi, Performance evaluation of waste iron shavings (Fe^0) for catalytic ozonation in removal of sulfamethoxazole from municipal wastewater treatment plant effluent in a batch mode pilot plant, Chem. Eng. J., 383 (2020) 123093, doi: 10.1016/j.cej.2019.123093.
[91] M.C. Tonucci, L.V.A. Gurgel, S.F. de Aquino, Activated carbons from agricultural by-products (pine tree and coconut shell), coal, and carbon nanotubes as adsorbents for removal of sulfamethoxazole from spiked aqueous solutions: kinetic and thermodynamic studies, Ind. Crops Prod., 74 (2015) 111–121.